

# MAPPING HIPPOCAMPAL ATROPHY WITH A MULTI-SCALE MODEL OF SHAPE

Xinyang Liu<sup>1</sup>, Yonggang Shi<sup>2</sup>, Jonathan Morra<sup>2</sup>, Xiuwen Liu<sup>3</sup>, Paul Thompson<sup>2</sup>, Washington Mio<sup>1</sup>

<sup>1</sup>Department of Mathematics, Florida State University, Tallahassee, FL 32306

<sup>2</sup>Laboratory of NeuroImaging, UCLA School of Medicine, Los Angeles, CA 90095

<sup>3</sup>Department of Computer Science, Florida State University, Tallahassee, FL 32306

## ABSTRACT

We construct a multi-scale model of shape of surfaces in 3D space based on the heat kernel associated with the Laplace-Beltrami operator. The model is applied to the analysis of longitudinal neuroimaging data collected by the Alzheimer's Disease Neuroimaging Initiative. We use measures of shape deformation energy to quantify, compare and create maps of regional changes in hippocampal shape in normal aging, progression of Alzheimer's disease and mild cognitive impairment over a one-year period.

**Index Terms**— Shape space, heat kernel, hippocampal atrophy, Alzheimer's disease, ADNI.

## 1. INTRODUCTION

We introduce a 1-parameter family of shape metrics derived from a multi-scale representation of parametric surfaces in 3D space based on the heat kernel. The metrics and the associated deformation energies are applied to the analysis and comparison of relative changes in hippocampal shape and size over a 1-year period in normal (NL) aging, progression of Alzheimer's disease (AD), and subjects diagnosed with mild cognitive impairment (MCI). MCI is regarded as a transitional stage to AD. The analysis relies on longitudinal data collected by the Alzheimer's Disease Neuroimaging Initiative (ADNI), a large multi-site study of 800 elderly subjects [1]. This paper is based on magnetic resonance (MR) scans of the brain acquired at two time points, one year apart, of a subset of 425 subjects classified according to the baseline diagnoses as follows: 134 NL, 211 MCI, and 80 AD. We use the proposed shape metrics to quantify regional shape dissimilarity and to create statistical maps that identify specific areas of the contour surface of the hippocampus (HC) where differences in anatomical characteristics of the aforementioned dynamical processes are most salient according to the model. Changes in hippocampal shape and volume due to neurodegeneration in AD are well documented in the literature and have been approached with a variety of methods such as measures of

radial compression and tensor-based morphometry; cf. [2, 3] and references therein.

The proposed approach to shape may be viewed as a continuous extension to surfaces of the classical Procrustes analysis of shape [4]. As in [5], the model is based on a first-order parametric representation, not just on the positions of points in 3D space. First-order metrics are of interest because they are more sensitive to non-linear deformations such as those associated with tissue loss in the hippocampus. However, unlike [5], the model is sensitive to size and the first-order term in the metric is smoothed out with the Riemannian heat kernel allowing us to suppress noise and focus on robust first-order differences at the most relevant scales. The shape metric is also employed in the construction of anatomical atlases as sample mean shapes. We use a hippocampal atlas as a reference anatomy for the parametric model, as well as a common domain for the analysis and comparison of measures of 1-year shape variation in different subjects and groups.

The hippocampi of all subjects were segmented from MR volumes with the techniques of [2]. A triangle mesh was constructed to represent the contour surface of each segmented hippocampus. Following a standard practice, we chose the baseline scan of one of the normal subjects as a reference and registered all other meshes with the reference mesh  $M$  using the direct mapping method of [6]. All surfaces were re-meshed by transferring the mesh structure of the reference shape via the correspondences, so that they are all equipped with compatible triangulations and parametrized over  $M$ .

The continuous shape model is developed in Section 2 and the discretization in Section 3. The construction of atlases is discussed in Section 4, which is followed by applications to ADNI data in Section 5, a summary and discussion.

## 2. A MULTI-SCALE MODEL OF SHAPE

Let  $M$  be a closed, connected surface with a fixed Riemannian metric; that is, a surface whose tangent space  $T_p M$  at each point  $p$  is equipped with an inner product  $\langle \cdot, \cdot \rangle_p$  that varies smoothly with  $p$ . A parametric 3D shape modeled on  $M$  is represented by a mapping  $\alpha: M \rightarrow \mathbb{R}^3$ , where  $\mathbb{R}^3$  denotes 3D Euclidean space. As in conventional Procrustes analysis, we center  $\alpha$  by translating it so that  $\int_M \alpha(p) d\sigma(p) = 0$ ,

This research was supported in part by NSF grants DMS-0713012 and CCF-0514743, and NIH Roadmap for Medical Research grant U54 RR021813.

where  $d\sigma$  is the area element of  $M$ .

Let  $\Delta_M$  be the Laplace-Beltrami operator on  $M$  and  $K(p, q, t)$  the associated heat kernel,  $p, q \in M$  and  $t > 0$ . If  $0 = \lambda_0 < \lambda_1 \leq \lambda_2 \leq \dots$  are the eigenvalues of  $-\Delta_M$  with orthonormal eigenfunctions  $\phi_i: M \rightarrow \mathbb{R}$ ,  $i \geq 0$ , then

$$K(p, q, t) = \sum_{i=0}^{\infty} e^{-\lambda_i t} \phi_i(p) \phi_i(q), \quad (1)$$

cf. [7]. Given  $\alpha: M \rightarrow \mathbb{R}^3$ , let

$$\alpha(p, t) = \int_M K(p, q, t) \alpha(q) d\sigma(q). \quad (2)$$

$\alpha(\cdot, t)$ ,  $t > 0$ , gives as a scale-space representation of the shape  $\alpha$ . As  $t$  increases, the representation smoothes out the shape by dampening the high frequency terms exponentially. The derivative of  $\alpha(p, t)$  with respect to the variable  $p$  is a linear mapping  $d\alpha_{(p,t)}: T_p M \rightarrow \mathbb{R}^3$ . We adopt the inner product of linear mappings  $P, Q: T_p M \rightarrow \mathbb{R}^3$  given by  $\langle P, Q \rangle_p = \text{trace}(Q^* P)$ , where,  $Q^*$  is the adjoint of  $Q$ . For each  $t > 0$ , we consider the Sobolev-type inner product

$$\begin{aligned} \langle \alpha, \beta \rangle_t &= a \int_M \alpha(p) \cdot \beta(p) d\sigma(p) \\ &+ b \int_M \langle d\alpha_{(p,t)}, d\beta_{(p,t)} \rangle_p d\sigma(p), \end{aligned} \quad (3)$$

where  $a, b > 0$ . Note that the heat kernel is only used on the second term. As in Kendall's formulation [4] and the Sobolev model of [5], we could also normalize size with respect to the proposed metric. However, as one of our goals is to use the metric to detect change in shape and size due to hippocampal atrophy, we do not normalize size. As usual, we account for shape invariance under change of orientation via the action of the group  $O(3)$  of  $3 \times 3$  orthogonal matrices. If  $s_\alpha, s_\beta$  are the shapes represented by  $\alpha$  and  $\beta$ , the  $t$ -distance is defined as

$$d_t(s_\alpha, s_\beta) = \min_{U \in O(3)} \|\alpha - U \circ \beta\|_t, \quad (4)$$

where  $\|\cdot\|_t$  is the norm associated with (3) and  $\circ$  denotes composition of mappings. One can calculate explicitly the orthogonal mapping  $\hat{U}$  that realizes the shape distance. Write the components of  $\alpha$  as  $(\alpha_1, \alpha_2, \alpha_3)$  and similarly for  $\beta$ . Let  $A$  be the  $3 \times 3$  matrix whose  $(i, j)$ -entry is

$$\begin{aligned} a_{ij} &= a \int_M \alpha_i(p) \beta_j(p, t) d\sigma(p) \\ &+ b \int_M \langle \nabla_M \alpha_i(p, t), \nabla_M \beta_j(p, t) \rangle_p d\sigma(p), \end{aligned} \quad (5)$$

where  $\nabla_M$  denotes the Riemannian gradient. If  $A = V_1 \Sigma V_2^T$  is a singular value decomposition (SVD) of  $A$ , then  $\hat{U} = V_1 V_2^T$ . Letting  $\hat{\beta} = \hat{U} \circ \beta$ , (3) and (4) imply that

$$\begin{aligned} d_t^2(s_\alpha, s_\beta) &= a \int_M \|\alpha(p) - \hat{\beta}(p)\|^2 d\sigma(p) \\ &+ b \int_M \|d\alpha_{(p,t)} - d\hat{\beta}_{(p,t)}\|_p^2 d\sigma(p). \end{aligned} \quad (6)$$

If we view  $d_t^2(s_\alpha, s_\beta)$  as a deformation energy, then (6) expresses the energy as the integral of local contributions. Thus, we define the energy function  $E_{\alpha, \beta}^t: M \rightarrow \mathbb{R}$  by

$$E_{\alpha, \beta}^t(p) = a \|\alpha(p) - \hat{\beta}(p)\|^2 + b \|d\alpha_{(p,t)} - d\hat{\beta}_{(p,t)}\|_p^2. \quad (7)$$

The local energy  $E_{\alpha, \beta}^t(p)$  quantifies how much the shapes of  $\alpha$  and  $\beta$  differ at  $p$  from the standpoint of the metric  $d_t$ .

### 3. THE DISCRETE MODEL

In the discrete model, the reference surface  $M$  becomes a triangle mesh whose vertex and edge sets are denoted  $V = \{v_0, v_1, v_2, \dots, v_n\}$  and  $E = \{e_1, e_2, \dots, e_m\}$ , respectively. The discrete analogue of a Riemannian structure on  $M$  is a prescription of edge lengths. We let  $\ell_j$  be the length of the edge  $e_j$ . Once the edge lengths are known, other metric quantities such as areas are also prescribed. A parametric shape  $\alpha$  is represented by a piecewise linear map  $M \rightarrow \mathbb{R}^3$ . Therefore  $\alpha$  is determined by the values it takes on the vertices of  $M$ . Thus, we write  $\alpha$  as the  $n \times 3$  matrix whose  $i$ th row is  $\alpha(v_i)$ . To define the discrete derivative, we fix an orientation for each edge  $e_j$ . The derivative of  $\alpha$  is defined on  $E$  by  $d\alpha(e_j) = [\alpha(e_j^+) - \alpha(e_j^-)] / \ell_j$ , where  $e_j^+$  and  $e_j^-$  are the terminal and initial vertices of  $e_j$ , respectively. The Laplace-Beltrami operator is discretized as in [8, 9] and its eigenvalues  $0 = \lambda_0 < \lambda_1 \leq \dots \leq \lambda_n$  and corresponding eigenvectors  $\phi_0, \phi_1, \dots, \phi_n$  are calculated with the method of [9]. The heat kernel is defined as in (1), except that the sum is finite. The discrete form of (2) is

$$\alpha(v_i, t) = \sum_{\ell=0}^n \sum_{j=1}^n e^{-\lambda_\ell t} \phi_\ell(v_i) \phi_\ell(v_j) \alpha(v_j) A_j, \quad (8)$$

where  $A_j$  is the area of the star neighborhood of  $v_j$  in the first barycentric subdivision of  $M$ . To further smooth out the shape, we often truncate this sum at the  $r$ th eigenvalue,  $r$  small, so that the index  $\ell$  only ranges from 0 to  $r$ . We can now discretize the inner product (3) as

$$\begin{aligned} \langle \alpha, \beta \rangle_t &= a \sum_{i=0}^n \alpha(v_i) \cdot \beta(v_i) A_i \\ &+ b \sum_{j=1}^m d\alpha(e_j, t) \cdot d\beta(e_j, t) B_j, \end{aligned} \quad (9)$$

where  $B_j$  is the local area around  $e_j$ , that is, the sum of the areas of the two triangles determined by the edge  $e_j$  and the barycenters of the triangles adjacent to  $e_j$ . Lastly, a calculation shows that the natural discretization of the local energy  $E_{\alpha, \beta}$  in (7) as a function defined on the vertex set  $V$  is

$$\begin{aligned} E_{\alpha, \beta}^t(v_i) &= a \|\alpha(v_i) - \hat{\beta}(v_i)\|^2 \\ &+ \frac{b}{2A_i} \sum_j \|d\alpha(e_j, t) - d\hat{\beta}(e_j, t)\|^2 B_j, \end{aligned} \quad (10)$$

where  $j$  varies over the indexes of the edges incident with  $v_i$ .

#### 4. HIPPOCAMPAL ATLAS

We denote by  $[\alpha]$  the shape associated with a piecewise linear mapping  $\alpha: M \rightarrow \mathbb{R}^3$ . Let  $[\alpha_1], \dots, [\alpha_r]$  be a family of shapes, with each  $\alpha_i$  centered. The *Fréchet mean shape*  $[\bar{\alpha}]$  of the family, with respect to the metric  $d_t$ , is a shape that minimizes the scatter function

$$V_t([\alpha]) = \frac{1}{2} \sum_{i=1}^r d_t^2([\alpha], [\alpha_i]) = \frac{1}{2} \sum_{i=1}^r \|\alpha - U_i(\alpha) \circ \alpha_i\|_t^2,$$

where  $U_i(\alpha)$  is the orthogonal transformation that optimally aligns  $\alpha_i$  with  $\alpha$ . A gradient calculation shows that, at a minimum of  $V$ ,  $\alpha$  must satisfy  $\frac{1}{r} \sum_{i=1}^r U_i(\alpha) \circ \alpha_i = \alpha$ . Thus, we are interested in fixed points of the mapping  $T(\alpha) = \sum_{i=1}^r U_i(\alpha) \circ \alpha_i / r$ . In analogy with [10], we approach this problem with an algorithm that is based on the assumption that the fixed point of  $T$  is a local attractor and the samples form a compact cluster in shape space. We initialize the search with one of the given shapes, say,  $\alpha = \alpha_1$ . Then, we update  $\alpha$  according to  $\alpha_{\text{new}} = T(\alpha)$  until convergence. As



Fig. 1. Atlases of the left and right hippocampi.

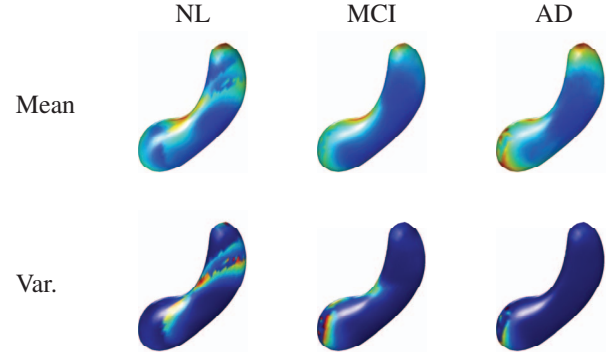
explained in the Introduction, all hippocampal surfaces are parametrized over a reference mesh. Fig. 1 shows atlases of the left and right hippocampi constructed as the mean shapes of all 134 control samples. We used a representation with 300 eigenfunctions and  $t = 0.01$ , and a metric with  $a = 0.9$  and  $b = 0.1$ . By construction, all surfaces are also registered with the atlas.

#### 5. HIPPOCAMPAL ATROPHY

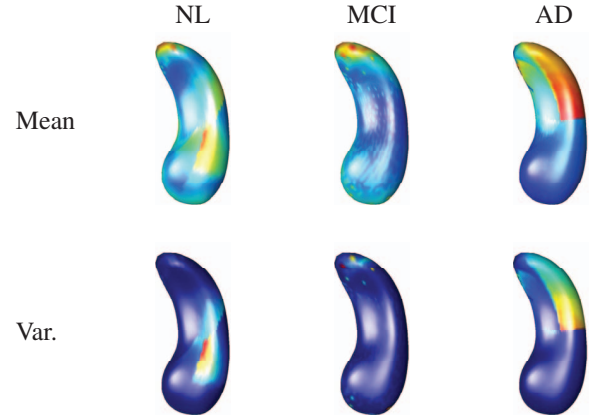
We describe our analysis of the shape of the left HC, but the same procedure was applied to the right HC. We also replace the domain  $M$  of all parametrizations with the atlas constructed in Section 4. We index the subjects with  $i$ ,  $1 \leq i \leq 425$ , and separate them into 3 groups labeled NL, MCI, and AD according to the baseline diagnoses. The sets of indexes associated with the subjects in the NL, MCI, and AD groups are denoted  $I_{\text{NL}}$ ,  $I_{\text{MCI}}$ , and  $I_{\text{AD}}$ , respectively.

As we are interested in comparing relative shape change over one year, we first scale the baseline surface of each individual so that the first non-zero eigenvalue of  $-\Delta$  is  $\lambda_1 = 1$  and apply the same scale factor to the follow-up surface. For the subject labeled  $i$ , we compute the energy function of the deformation from baseline to follow-up, as defined in (7),

which we denote simply by  $E_i: M \rightarrow \mathbb{R}$ . Recall that  $E_i(p)$  quantifies the local contribution near  $p$  to the total deformation energy. Fig. 2 (a) shows plots of the mean energy functions and variances for the left hippocampus of the NL, MCI, and AD groups. Fig. 2 (b) shows analogous plots for the right hippocampus. The views differ slightly to highlight the regions where shape deformation over 1 year is most salient. Note that shape change is not uniformly distributed, especially on the right hippocampus of the AD group. The color



(a) Left Hippocampus



(b) Right Hippocampus

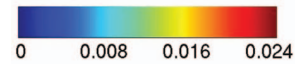


Fig. 2. Plots of the mean energy functions and variances for the left and right hippocampi of the NL, MCI, and AD groups.

scale shown in Figure 2 applies to the mean energy in all cases, except for the right hippocampus of the AD group, where the range of values is 0.00–0.13.

Now we compare the energy functions of the subjects in the NL group with those in the MCI and AD groups, respectively, in order to quantify and characterize regional differ-

ences in normal aging over a 1-year period with morphological changes in MCI and progression of AD. We discuss the NL-AD comparison, but the same method was applied to NL-MCI.

For each  $p \in M$ , we examine the distribution of the values  $E_i(p)$ ,  $i \in I_{NL}$ , of the energy functions for NL subjects and compare it with the distribution of  $E_i(p)$ ,  $i \in I_{AD}$ . Since we are particularly interested in capturing neurodegeneration, in which case the deformation energy is expected to be larger, we apply a 1-tailed  $t$ -test to compare the two groups. Fig. 3 shows p-value maps that highlight the regions where differences on the hippocampus are significant.

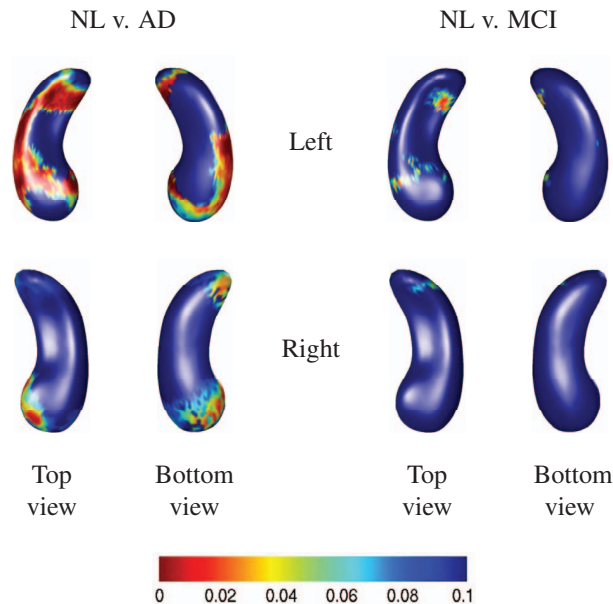


Fig. 3. P-value maps of normal aging versus MCI and AD.

## 6. SUMMARY AND DISCUSSION

We developed a multi-scale model of shape of surfaces in 3D space based on a heat-kernel representation derived from the Laplace-Beltrami operator. The model was applied to the comparison of hippocampal shape changes in normal aging, progression of Alzheimer’s disease, and mild cognitive impairment over a 1-year period using longitudinal data collected by the Alzheimer’s Disease Neuroimaging Initiative. Shape deformation energies were used to quantify regional morphological changes in the hippocampus under these three dynamical processes and to create maps that identify regions where significant group differences are detected by the model. The measures of shape evolution employed are solely based on the contour surface of the hippocampus. However, as the characterization of volume loss due to neurodegeneration is of primary interest in tracking the disease, in future work, we

will extend the model to the entire hippocampal volume to produce a model that is more sensitive to tissue loss.

## 7. REFERENCES

- [1] S.G. Mueller, M.W. Weiner, L.J. Thal, R.C. Petersen, C. Jack, W. Jagust, J.Q. Trojanowski, A. Toga, and L. Beckett, “The Alzheimer’s disease neuroimaging initiative,” *Clin. North Am.*, vol. 15, pp. 869–877 xi–xii, 2005.
- [2] J. Morra, Z. Tu, L.G. Apostolova et al., and the ADNI, “Automated mapping of hippocampal atrophy in 1-year repeat MRI data from 490 subjects with Alzheimer’s disease, mild cognitive impairment, and elderly controls,” *NeuroImage*, vol. 45(1 Suppl), pp. S3–15, 2009.
- [3] X.Hua, A.D. Leow, S. Lee, A.D. Klunder, A. Toga, and N. Lepore et al., “3D Characterization of brain atrophy in Alzheimer’s disease and mild cognitive impairment using tensor-based morphometry,” *NeuroImage*, vol. 41, pp. 19–34, 2008.
- [4] D.G. Kendall, “Shape manifolds, Procrustean metrics and complex projective spaces,” *Bull. London Math. Soc.*, vol. 16, pp. 81–121, 1984.
- [5] X. Liu, W. Mio, Y. Shi, I. Dinov, Xiuwen Liu, N. Lepore, F. Lepore, M. Fortin, P. Voss, M. Lassonde, and P. Thompson, “Models of normal variation and local contrasts in hippocampal anatomy,” *Lecture Notes In Computer Science*, vol. 5242, pp. 407–415, 2008.
- [6] Y. Shi, P.M. Thompson, G.I. de Zubizaray, S.E. Rose, Z. Tu, I. Dinov, and A.W. Toga, “Direct mapping of hippocampal surfaces with intrinsic shape context,” *NeuroImage*, vol. 37, no. 3, pp. 792–807, 2007.
- [7] S. Rosenberg, *The Laplacian on a Riemannian Manifold*, Cambridge University Press, 1997.
- [8] M. Desbrun, A. Hirani, M. Leok, and J. Marsden, “Discrete exterior calculus,” arXiv:math/0508341v2, 2005.
- [9] J. Bates, Y. Wang, X. Liu, and W. Mio, “Registration of contours of brain structures through a heat-kernel representation of shape,” *ISBI*, 2009.
- [10] S. Huckemann and H. Ziezold, “Principal component analysis for Riemannian manifolds, with an application to triangular shape spaces,” *Advances in Applied Probability*, vol. 38, pp. 299–319, 2006.